



Planar Superstructure Defects in Ordered Alloys with $L1_0$ Structure

A. R. Khalikov¹ · E. A. Korznikova^{1,2} · A. A. Kudreyko³ · Yu. V. Bebikhov⁴ · S. V. Dmitriev^{2,5}

Received: 17 June 2022 / Accepted: 25 September 2022

© The Author(s) under exclusive licence to The Korean Institute of Metals and Materials 2022

Abstract

The structure and energy of planar superstructure defects (PSDs) in ordered alloys with the $L1_0$ superstructure are analyzed using an approach based on the analysis of the translational and point symmetry of the structure and the summation of pairwise interatomic bonds across the defect plane. The symmetry analysis of the alloy revealed six superstructure domains and one antiphase vector. Analytical expressions are obtained for calculating the sublimation energy and the energy of an arbitrary PSD under the assumption of pairwise interatomic interactions and neglecting the tetragonality of the alloy and the relaxation of atoms due to the difference in the atomic radii of the components. An expression is derived for finding all possible planes of conservative antiphase boundaries. The presented results are useful for analyzing slip systems and classifying possible PSDs in $L1_0$ ordered alloys.

Keywords Ordered alloy · $L1_0$ superstructure · Planar superstructure defect · Antiphase boundary · Domain boundary · Energy of defect

1 Introduction

There are many binary and ternary alloys, which in a certain temperature range are ordered into the $L1_0$ superstructure based on the fcc lattice, see Fig. 1. Among them are the alloys containing magnetic elements Fe, Co and Ni, noble metals Cu and Au, as well as the light elements Ti and Al.

First of all, the fields of application of alloys with the $L1_0$ superstructure are described. Probably, magnetic $L1_0$ ordered alloys are of most interest for applications [1–5]. FePt alloy, due to its large perpendicular magnetocrystalline anisotropy, is a potential material for electrode for high-density

information storage devices [1]. Tetragonal martensite $L1_0$ phase can appear as an intermediate phase in phase transitions in Fe-Ga ferromagnetic shape memory alloys [6]. $L1_0$ TiAl has been studied as a high-temperature material because of its high melting temperature and low density [7].

Ordered alloys and compounds support phases with ordered vacancies. For instance, vacancy ordering in the carbon sublattice is observed in carbides of IV and V group transitional metals with $B1$ structure [8]. Copper-poor ordered vacancy compound $\text{Cu}(\text{In,Ga})\text{Se}_2$ can be used for high performance solar cells [9]. The first-principles density functional theory calculations reveal the stability of a family of ordered phases that combine features of $L1_2$ and $L1_0$ in different ratios and confirm the stability of vacancy ordered $B2$ derivatives that are stable in the Al-rich half of the phase diagram [10].

Ag or Pb can effectively promote the transition to the ordered state of $L1_0$ -FePt nanoparticles, which are used as catalysts [11–13]. The difference between the diffusion coefficients of Ag and Pb can generate a large number of vacancies in the lattice, which contribute to the rearrangement of Fe and Pt atoms.

Second, planar superstructure defects are defined and the mechanisms of their formation are described. A planar defect is called a superstructure defect if, on both sides of the plane of the defect, atoms remain in their lattice positions

✉ S. V. Dmitriev
dmitriev.sergey.v@gmail.com

¹ Ufa State Aviation Technical University, Ufa 450008, Russia

² Institute of Molecule and Crystal Physics, Ufa Federal Research Centre of Russian Academy of Sciences, Ufa 450075, Russia

³ Department of Medical Physics and Informatics, Bashkir State Medical University, Ufa 450008, Russia

⁴ Polytechnic Institute (Branch) in Mirny, North-Eastern Federal University, Mirny, Sakha Republic (Yakutia) 678170, Russia

⁵ Ufa State Petroleum Technological University, Ufa 450064, Russia

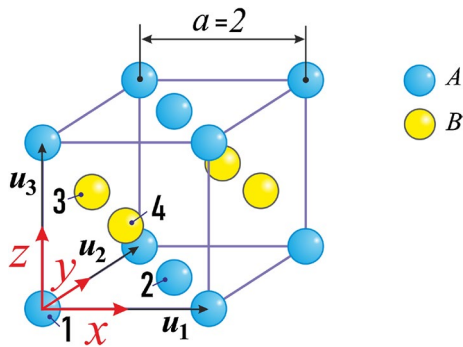


Fig. 1 A cubic translational cell of the $L1_0$ superstructure based on the fcc lattice. Atoms A and B are shown in blue and yellow, respectively. For convenience, for the lattice parameter $a = 2$ is set, then the translation vectors of the cubic lattice are $u_1 = (2, 0, 0)$, $u_2 = (0, 2, 0)$, $u_3 = (0, 0, 2)$. Cubic monatomic sublattices are numbered from 1 to 4. Sublattices 1 and 2 (3 and 4) are occupied by the atoms A (B)

(disregarding atomic relaxation near the defect due to the difference in atomic radii of the alloy components), but the arrangement of atoms on the shifted monatomic lattices changes [14]. Such defects are possible only in ordered alloys.

Planar superstructure defects (PSDs) are inevitably formed in the process of ordering by the mechanism of nucleation and growth as a result of the collision of different domains of the ordered phase [14]. They can also be formed as a result of dislocation glide [14]. APBs can be separated by interfacial boundaries as a result of the wetting phenomenon. Wetting ordered interlayers have been observed experimentally and simulated using the Ising model in a $L1_0$ alloy with a composition close to $Co_{40}Pt_{60}$ [15]. A macroscopic layer of $L1_2$ structure appears between orientational domain wall and a complex $L1_2/L1_0/L1_2$ structure with four interfaces separates the anti-phase domains [15].

Next, the effect of PSDs on the properties of $L1_0$ alloys is discussed. PSDs control many properties of the ordered alloys. For example, $L1_0$ ordered TiAl alloy exhibits a flow-stress anomaly with a maximum at approximately 600 °C, which is explained by the dislocation dissociation and formation of planar defects [16]. Superdislocations break up into a triplet that includes an antiphase boundary (APB) and an internal stacking fault. The screw dislocation undergoes a glissile-sessile transition with increasing temperature, and the octahedral slip is replaced by a cubic one. Cross slip on octahedral planes at room temperature explains the high-temperature flow stress peak in TiAl [16].

It has been proposed that the high coercivity in $L1_0$ FePd films is explained by pinning of magnetic domain walls by APBs and twin boundaries [17].

Molecular dynamics simulations have shown that γ -TiAl with $L1_0$ ordered structure has a higher radiation resistance against primary damage formation, as compared

to the disordered Ti-50 at%Al alloy [18]. A positive correlation between dislocation density and coercivity of $L1_0$ Mn-Al alloys was established in the work [19].

A theoretical study on the ordering kinetics of FePt nanoparticles during high temperature annealing has shown that the remaining APBs are the major obstacle in obtaining completely ordered nanoparticles [20].

A high degree of ordering of $L1_0$ alloys can be achieved not only by prolonged annealing. Highly ordered CoPt and NiPt nanoparticles with $L1_0$ structure were obtained at lower processing temperatures and shorter reaction times than ordinary thermal processes [21]. At high temperatures, an order-disorder phase transition usually occurs. Using in-situ synchrotron X-ray scattering it was shown that PtNi nanocrystals on sapphire substrate were ordered in the tetragonal $L1_0$ structure at low temperatures and at 640 °C a transition to the disordered fcc structure was observed [22].

The ordered $L1_0$ phase is tetragonal and anisotropic; this must be taken into account when evaluating the properties of single crystals, for example, diffusion coefficients, as was done in molecular dynamics studies for FePt alloy in the temperature range from 1300 to 1600 K [23]. The $L1_0$ tetragonal distortion of FeNi can be enhanced by introducing interstitial N-doping, which can control its magnetic properties [24].

Long-period superstructures with antiphase domains in the annealed nanocrystals of $L1_0$ -ordered CoPt alloy have been observed by high-resolution transmission electron microscopy in form of a checkerboard pattern [25].

Finally, various modeling methods used to study the structure and properties of $L1_0$ alloys are discussed. The time evolution of antiphase domains in $L1_0$ ordered Fe-Pd alloy was simulated based on the combination of the cluster variation method with the phase-field method [26–28].

Monte Carlo simulations of alloy ordering is often performed for rigid lattice, i.e., neglecting atomic relaxation [29]. Either the vacancy diffusion according to the Glauber algorithm or voxel Ising-type models can be used [29, 30]. Energies of PSDs in various superstructures were expressed in terms of pair interatomic potentials [31, 32].

Generalized Ginzburg-Landau approach was used to formulate the statistical theory of equilibrium antiphase and interphase boundaries for the B2 and $L1_0$ ordered alloys [33].

Ab-initio simulation method was used to calculate the energies of APBs in Al-rich γ -TiAl alloys with $L1_0$ superstructure. The relaxed APB energies for type-A and type-C APBs were found to be 15.44 and 124.16 mJ/m², respectively [34]. In Al_5Ti_3 alloy, type-A and type-C APBs are most common. This alloy is an Al-rich derivative of the γ -TiAl phase with $L1_0$ order. In the work [35], the Monte Carlo simulation of the ordering kinetics has been performed and the expressions for the energies of type-A and type-C APBs have been given in terms of pair interaction energies.

Theoretical studies of the structure and properties of ordered alloys began in the middle of the last century [14, 36–38]. In these and subsequent works, the theory of interphase and antiphase boundaries in fcc and bcc ordered alloys was developed on the basis of an analysis of the symmetry of alloys and assumptions about pair interactions and rigid coordination spheres. In this work, a similar approach and similar assumptions are used to simplify the problem and make it possible to obtain analytical expressions for the PSD energy. The calculation of the PSD energy is reduced to the summation of pair interactions across the plane of the defect. Symmetry analysis is used to describe all possible types of PSDs in the $L1_0$ superstructure and to obtain a list of crystallographic planes in which conservative APBs are possible.

It can be seen that PSDs constitute an important class of defects in ordered alloys. A systematic analysis of the structure and energy of such defects in $L1_0$ ordered alloys has not been done. An analysis of the structure and energy of the PSDs for the family of ternary X_2YZ Heusler alloys was recently carried out [39]. In the present study, a similar analysis is carried out for alloys with the $L1_0$ superstructure.

2 Structure of the Alloy

This section describes the $L1_0$ packing of atoms in a binary alloy of stoichiometric composition AB based on the fcc lattice. The tetragonality of the lattice is neglected for simplicity. Let the cubic translational cell shown in Fig. 1 in the Cartesian coordinate system xyz , has the lattice parameter a . It is convenient to carry out a crystallographic analysis of the alloy by taking $a = 2$; in this case, all the coordinates of the atoms will be expressed in whole numbers. Atoms of the $L1_0$ superstructure occupy the sites of the fcc lattice. This superstructure is a union of four monatomic simple cubic lattices, two of which are occupied by A atoms, and the other two by B atoms. Atoms A and B are shown in Fig. 1 in blue and yellow, respectively.

First, the lattice L as a set of points in three-dimensional space with radius vectors

$$\mathbf{x} = \sigma_1 \mathbf{u}_1 + \sigma_2 \mathbf{u}_2 + \sigma_3 \mathbf{u}_3, \tag{1}$$

is defined, where $\sigma_i, i = 1, 2, 3$, are any integers and \mathbf{u}_i are three linearly independent vectors defining the basis of the lattice.

Simple cubic lattice L^c with the lattice parameter $a = 2$ is generated by the vectors

$$\mathbf{u}_1 = (2, 0, 0), \quad \mathbf{u}_2 = (0, 2, 0), \quad \mathbf{u}_3 = (0, 0, 2). \tag{2}$$

The superstructure $L1_0$, as noted above, can be defined as a union of 4 monatomic cubic lattices L^c (numbered by index

$m = 1, 2, 3, 4$) shifted by vectors $\boldsymbol{\mu}_m$, with atoms of sort S_m occupying the points of the m -th shifted lattice:

$$Q = \bigcup_{m=1}^4 (L^c + \boldsymbol{\mu}_m)_{S_m}, \tag{3}$$

where the shift vectors are

$$\begin{aligned} \boldsymbol{\mu}_1 &= (0, 0, 0), & \boldsymbol{\mu}_2 &= (1, 1, 0), \\ \boldsymbol{\mu}_3 &= (0, 1, 1), & \boldsymbol{\mu}_4 &= (1, 0, 1). \end{aligned} \tag{4}$$

The shifted cubic lattices are occupied by the atoms of sorts A and B as follows (see Fig. 1):

$$S_1 = A, \quad S_2 = A, \quad S_3 = B, \quad S_4 = B. \tag{5}$$

Expressions from (2) to (5) define the $L1_0$ superstructure as a union of 4 monatomic cubic lattices.

3 Sublimation Energy of the Alloy

The sublimation energy is the energy required to evaporate the crystal (to break all interatomic bonds). It is assumed that the interatomic interactions are described by pairwise potentials $\varphi_{S_i S_j}(r)$, where φ is the interaction energy of atoms of sorts S_i and S_j located at a distance of r . Here the superstructure $L1_0$ defined by (2–5) is considered. The sublimation energy of the superstructure Q per unit volume can be written as follows:

$$\begin{aligned} E &= \frac{1}{|U|} \sum_{\substack{i,j=1 \\ i > j}}^4 \sum_{\sigma_1, \sigma_2, \sigma_3 = -\infty}^{+\infty} \varphi_{S_i S_j}(|\mathbf{A}|) \\ &+ \frac{1}{2|U|} \sum_{i=1}^4 \left[-\varphi_{S_i S_i}(0) + \sum_{\sigma_1, \sigma_2, \sigma_3 = -\infty}^{+\infty} \varphi_{S_i S_i}(|\mathbf{B}|) \right], \end{aligned} \tag{6}$$

where

$$\begin{aligned} \mathbf{A} &= \sigma_1 \mathbf{u}_1 + \sigma_2 \mathbf{u}_2 + \sigma_3 \mathbf{u}_3 + \boldsymbol{\mu}_i - \boldsymbol{\mu}_j, \\ \mathbf{B} &= \sigma_1 \mathbf{u}_1 + \sigma_2 \mathbf{u}_2 + \sigma_3 \mathbf{u}_3. \end{aligned} \tag{7}$$

In Eq. (6), the first line is the interaction energy of monatomic shifted lattices, and the second line is the interaction energy of atoms in the monatomic shifted lattices. $|U| = a^3 = 8$ is the volume of a primitive translation cell, which can be calculated as the determinant of the U matrix, the rows of which contain the Cartesian coordinates of the vectors \mathbf{u}_i given by (2). In practice, the limits of summation over the indices σ_i are finite, sufficient to take into account all interactions within the cutoff radius of the potentials.

Expanding the sums in Eq. (6), the sublimation energy of the alloy per unit volume is expressed through pair

potentials, taking into account interactions up to the 8th coordination sphere

$$\begin{aligned}
 E = \frac{1}{a^3} & \left[4\varphi_{AA}(R_1) + 16\varphi_{AB}(R_1) + 4\varphi_{BB}(R_1) \right. \\
 & + 6\varphi_{AA}(R_2) + 6\varphi_{BB}(R_2) \\
 & + 8\varphi_{AA}(R_3) + 32\varphi_{AB}(R_3) + 8\varphi_{BB}(R_3) \\
 & + 12\varphi_{AA}(R_4) + 12\varphi_{BB}(R_4) \\
 & + 8\varphi_{AA}(R_5) + 32\varphi_{AB}(R_5) + 8\varphi_{BB}(R_5) \\
 & + 8\varphi_{AA}(R_6) + 8\varphi_{BB}(R_6) \\
 & + 16\varphi_{AA}(R_7) + 64\varphi_{AB}(R_7) + 16\varphi_{BB}(R_7) \\
 & \left. + 6\varphi_{AA}(R_8) + 6\varphi_{BB}(R_8) \right], \quad (8)
 \end{aligned}$$

here R_i are the coordination sphere radii [40]:

$$\begin{aligned}
 R_1 = a/\sqrt{2}, \quad R_2 = a, \quad R_3 = a\sqrt{3}/2, \quad R_4 = a\sqrt{2}, \\
 R_5 = a\sqrt{5}/2, \quad R_6 = a\sqrt{3}, \quad R_7 = a\sqrt{7}/2, \quad R_8 = 2a. \quad (9)
 \end{aligned}$$

From the expression (8) it follows that, within first eight coordination spheres, on the odd coordination spheres the bonds AA , AB , and BB contribute to the sublimation energy, while on the even spheres, the contribution appears only from the AA and BB bonds.

4 Energetically Equivalent but Geometrically Different Representations of the $L1_0$ Superstructure

Here it is assumed that the $L1_0$ superstructure is defined by Eqs. (2-5).

Symmetry operations applied to the $L1_0$ superstructure, such as shifts by a lattice vector or point symmetry transformations of the cubic lattice, do not change the mutual arrangement of atoms and, therefore, do not change the sublimation energy. Here all possible geometrically different representations of the $L1_0$ superstructure that have the same sublimation energy will be found. To do this, first the shifts along the lattice vectors μ_i , $i = 1, 2, 3, 4$ defined by Eq. (4), and then 48 point symmetry transformations of the cubic lattice [41] are applied to the $L1_0$ superstructure. Note that taking into account the symmetry of the lattice helps to solve

Table 1 Change in the atomic sorts of four cubic shifted lattices of the $L1_0$ superstructure, defined by Eqs. (2-5) as a result of the shifts by the vectors μ_i , $i = 1, 2, 3, 4$

Shift vectors	$\mu_1 = (0, 0, 0), \quad \mu_2 = (1, 1, 0)$
S_i after shift	$ABBA$
Shift vectors	$\mu_3 = (0, 1, 1), \quad \mu_4 = (1, 0, 1)$
S_i after shift	$BBAA$

Table 2 Change in the atomic sorts of four cubic shifted lattices of the $L1_0$ superstructure, defined by Eqs. (2-5) as a result of point symmetry transformations

Transformation	Rotation of $ABBB$ by $\pi/2$ about x axis
S_i after transformation	$ABBA$
Transformation	Rotation of $ABBB$ by $\pi/2$ about y axis
S_i after transformation	$ABAB$
Transformation	Rotation of $BBAA$ by $\pi/2$ about x axis
S_i after transformation	$BAAB$
Transformation	Rotation of $BBAA$ by $\pi/2$ about y axis
S_i after transformation	$BABA$

various problems, for example, to find exact dynamic solutions of the equations of motion of atoms in crystals [42].

The first step is the analysis of the shifts along the lattice vectors. In Table. 1 the change in the sorts of atoms of four cubic shifted lattices, S_i , is shown for the shift vectors μ_j , given by Eq. (4). The shifts are performed according to $(\mu_m - \mu_j) \bmod(2)$, that is, the components of the vectors after subtraction are returned to the volume of a cubic translational cell with a lattice parameter $a = 2$. It can be seen from Table. 1 that the shift by the vectors μ_1 and μ_2 do not change the arrangement of the atom sorts. On the other hand, the shifts by the vectors μ_3 and μ_4 swap the atom sorts A and B .

Application of the 48 point symmetry transformations of the cubic lattice reveals energetically equivalent representations of the $L1_0$ superstructure different from those shown in Table. 1.

In Fig. 2 all possible energetically equivalent and geometrically different representations of the $L1_0$ superstructure are shown. In panels (a) and (b) the structures listed in Tab. 1 are

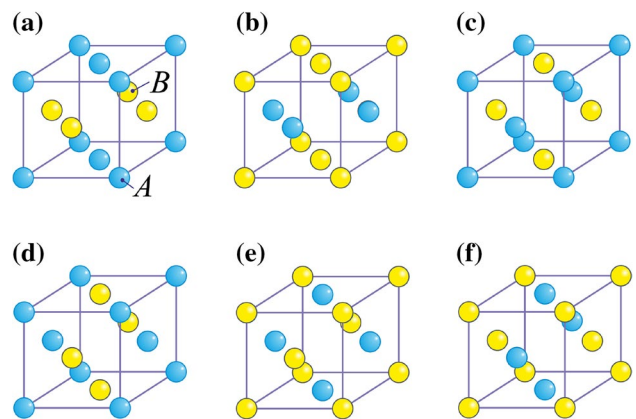


Fig. 2 All possible arrangements of A and B atoms on the shifted cubic lattices in the $L1_0$ superstructure obtained by the lattice vector shifts and point symmetry transformations: **a** $ABBA$, **b** $BBAA$, **c** $ABBA$, **d** $ABAB$, **e** $BAAB$ and **f** $BABA$. This is a complete list of possible domains in the $L1_0$ superstructure

shown, while other structures are listed in Tab. 2. Structures (a) and (b) can be transformed one to another by the lattice vector shift. The same is true for the structures (c) and (d), as well as for the structures (d) and (f). Structures (a) and (c) can be transformed one to another by the rotation by $\pi/2$ about x axis. Structures (a) and (d) can be transformed one to another by the rotation by $\pi/2$ about y axis. Structures (b) and (e) can be transformed one to another by the rotation by $\pi/2$ about x axis. Structures (b) and (f) can be transformed one to another by the rotation by $\pi/2$ about y axis.

5 Analysis of Possible Types of Planar Superstructure Defects in $L1_0$

With the results obtained in Sec. 4 one can describe all possible PSDs in the $L1_0$ superstructure. The plane of a PSD separates geometrically different but energetically equivalent representations of the $L1_0$ superstructure. Antiphase boundaries and C -domains should be distinguished. A conservative antiphase boundary (CAPB) separates two domains which can be superposed by a shift by a lattice vector parallel to the defect plane. A non-conservative antiphase boundary (NCAPB) is formed if the shift vector cannot be parallel to the defect plane. C -domain boundary separates two domains which can be superimposed by the rotation by the angle $\pi/2$. In some cases a shift by the lattice vector is required after the rotation.

Domains $AABB$ and $BBAA$ produce CAPB or NCAPB since they can be superposed by a shift by a lattice vector. The same is true for domains $ABBA$ and $BAAB$, as well as for domains $ABAB$ and $BABA$.

Domain $AABB$ (or $BBAA$) together with any domain except for $BBAA$ (or $AABB$) produce a C -domain. Similarly, domain $ABBA$ (or $BAAB$) together with any domain except for $BAAB$ (or $ABBA$) produce a C -domain; and domain $ABAB$ (or $BABA$) together with any domain except for $BABA$ (or $ABAB$) produce a C -domain.

Figure 3(a) shows the defect-free $L1_0$ superstructure, while panels (b) to (f) show five different types of PSD with orientation (001); the defect plane is shaded. Below the defect plane in all cases the $AABB$ domain is placed. Above the defect one has the domain (a) $AABB$, (b) $BBAA$, (c) $ABAB$, (d) $BABA$, (e) $ABBA$ and (f) $BAAB$. According to the classification described above, in (b) NCAPB is seen, since the shift vector t superposing the two domains is not parallel to the defect plane. All other defects are C -domains. In (d) and (f) after the rotation by $\pi/2$ the shift by the vector t is applied.

As one can see, CAPB are not possible in the case of (001) orientation, but they are possible for (010) and (100) orientations, as will be shown later.

In Fig. 4(a) the defect-free $L1_0$ superstructure is shown. Panels (b) to (f) show five different types of PSD with orientation (100); the defect plane is shaded. To the left of the defect plane in all cases the $AABB$ domain is placed. To the right of the defect one has the domain (a) $AABB$, (b) $BBAA$, (c) $ABAB$, (d) $BABA$, (e) $ABBA$ and (f) $BAAB$. In (b) CAPB is realized, since the shift vector t is parallel to the defect plane. All other defects are C -domains. In (d) and (f) after the rotation by $\pi/2$ the shift by the vector t is applied.

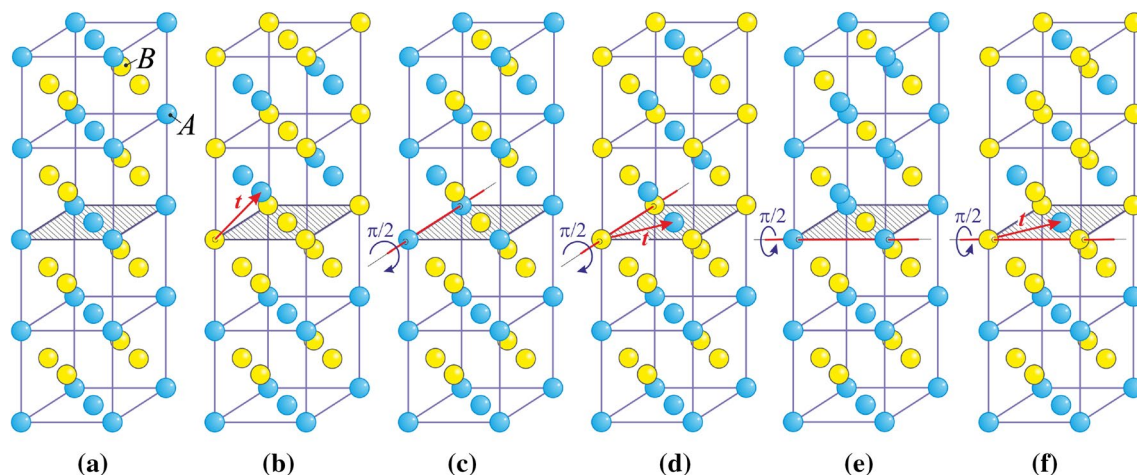
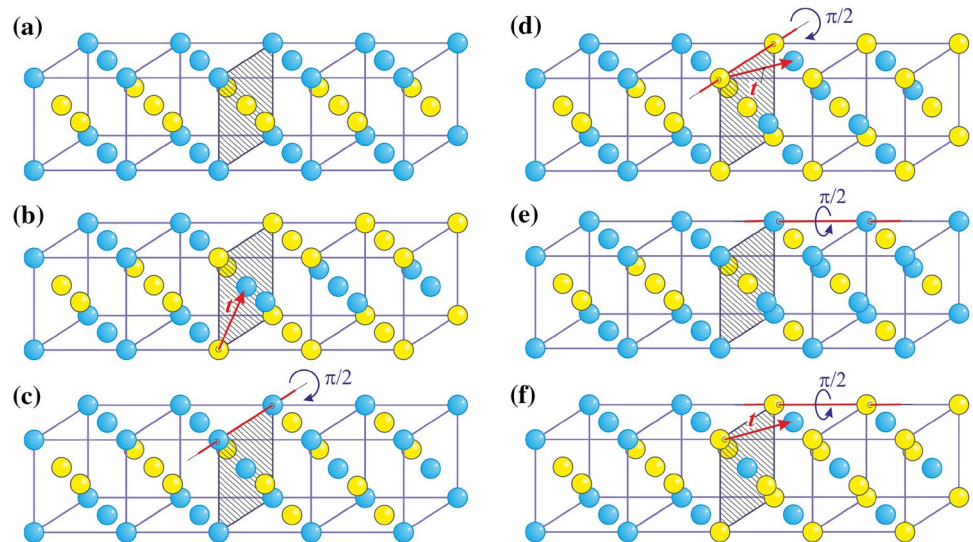


Fig. 3 a Defect-free $L1_0$ superstructure. (b-f) PSDs with orientation (001) obtained by substituting the upper half-space with geometrically different representations of $L1_0$ superstructure (the defect plane

is shaded). Below the defect plane in all cases the $AABB$ domain is placed. Above the defect one has the domains **b** $BBAA$, **c** $ABAB$, **d** $BABA$, **e** $ABBA$ and **f** $BAAB$

Fig. 4 **a** Defect-free $L1_0$ superstructure. PSD with orientation (100) obtained by substituting the right half-space with geometrically different representations of $L1_0$ superstructure (the defect plane is shaded). The **AABB** domain is located to the left of the defect plane in all cases. To the right of the defect one has the domains **b** **BBAA**, **c** **ABAB**, **d** **BABA**, **e** **ABBA** and **f** **BAAB**



6 Energy of Planar Superstructure Defects

In this section, the energy of an arbitrary PSD will be calculated under the assumption of pairwise interatomic interactions and without taking into account the tetragonality of the $L1_0$ alloy and atomic relaxation near the defect. Equations (2) to (5) define the $L1_0$ superstructure, and the defect plane has Miller indices (h, k, l) .

The PSD energy will be calculated by summing the energies of the atomic planes parallel to the plane of the defect. This is realized through the choice of the new translation vectors $\tilde{\mathbf{u}}$, two of which are parallel to the defect plane. For definiteness, let $\tilde{\mathbf{u}}_1$ and $\tilde{\mathbf{u}}_2$ be parallel to the defect plane. The third translation vector of the primitive cell of the $L1_0$ alloy should be chosen such that the volume of the translational cell of the lattice L^c is unchanged.

A two-dimensional lattice P defined by the translation vectors $\tilde{\mathbf{u}}_1$ and $\tilde{\mathbf{u}}_2$ is considered. Using the new basis, the superstructure Q is written as a union of atomic planes parallel to the defect:

$$Q = \bigcup_{m=1}^4 \bigcup_{\xi=-\infty}^{+\infty} (P + \boldsymbol{\mu}_m + \xi \tilde{\mathbf{u}}_3)_{S_m}, \quad (10)$$

where ξ is an integer index and $\boldsymbol{\mu}_m$ are the vectors (4).

Now the following two half-crystals terminated by the (h, k, l) plane are defined:

$$\begin{aligned} \tilde{Q}_- &= \bigcup_{m=1}^4 \bigcup_{\xi=-\infty}^{-1} (P + \boldsymbol{\mu}_m + \xi \tilde{\mathbf{u}}_3)_{S_m}, \\ \hat{Q}_+ &= \bigcup_{k=1}^4 \bigcup_{\xi=0}^{+\infty} (P + \boldsymbol{\mu}_k + \xi \tilde{\mathbf{u}}_3)_{S_k}. \end{aligned} \quad (11)$$

These half-crystals have $L1_0$ superstructure with different arrangement of atoms on the shifted sublattices S_m and S_k , there exist six such sublattices listed in Tables 1, 2: **AABB**, **BBAA**, **ABAB**, **BABA**, **ABBA** and **BAAB**. Index ξ in (11) ranges over negative and non-negative values in the half-crystals designated with the subscripts “-” and “+”, respectively. If $S_m = S_k$ then there is no defect and the defect does exist for $S_m \neq S_k$.

The PSD energy is calculated per unit area as the sum of three terms:

$$E = E(\tilde{Q}_- \leftrightarrow \hat{Q}_+) - \frac{E}{2}(\tilde{Q}_- \leftrightarrow \tilde{Q}_+) - \frac{E}{2}(\hat{Q}_- \leftrightarrow \hat{Q}_+). \quad (12)$$

The first term stands for the energy release per unit area as a result of joining of two half-crystals. The other two terms present the surface energy of these half-crystals. For example, to calculate the first term on the right side of (12), the interaction energies of two-dimensional packings on both sides of the defect plane are summed:

$$\begin{aligned} E(\tilde{Q}_- \leftrightarrow \hat{Q}_+) &= \frac{1}{|\tilde{\mathbf{u}}_1 \times \tilde{\mathbf{u}}_2|} \sum_{m=1}^4 \sum_{\xi=-\infty}^{-1} \sum_{k=1}^4 \sum_{\eta_1, \eta_2=-\infty}^{+\infty} \sum_{\eta_3=0}^{\infty} \varphi_{S_m S_k}(|\mathbf{r}|), \end{aligned} \quad (13)$$

where

$$\begin{aligned} \mathbf{r} = \mathbf{r}_{S_m} - \mathbf{r}_{S_k} &= (\boldsymbol{\mu}_m + \xi \tilde{\mathbf{u}}_3) - (\boldsymbol{\mu}_k + \eta_1 \tilde{\mathbf{u}}_1 \\ &+ \eta_2 \tilde{\mathbf{u}}_2 + \eta_3 \tilde{\mathbf{u}}_3), \end{aligned} \quad (14)$$

and the multiplier $|\tilde{\mathbf{u}}_1 \times \tilde{\mathbf{u}}_2|^{-1}$ normalizes the energy of the defect per unit area.

When calculating the energies $E(\tilde{Q}_- \leftrightarrow \tilde{Q}_+)$ and $E(\hat{Q}_- \leftrightarrow \hat{Q}_+)$ in (12), the expression (13) can be used taking $\varphi_{S_m S_m}(|\mathbf{r}|)$ and $\varphi_{S_k S_k}(|\mathbf{r}|)$, respectively, instead of $\varphi_{S_m S_k}(|\mathbf{r}|)$.

Here PSDs with orientations (001) and (100) are considered. The results will be presented in terms of ordering energies $\omega_{S_m S_k}$ and energy parameters $\Delta_{S_m S_k}$, defined as follows:

$$\begin{aligned}\omega_{AB}(R) &= \varphi_{AA}(R) + \varphi_{BB}(R) - 2\varphi_{AB}(R), \\ \Delta_{AB}(R) &= \varphi_{AA}(R) - \varphi_{BB}(R),\end{aligned}\quad (15)$$

where R is the radius of a coordination sphere (9).

6.1 Defects in the (001) Plane

For this defect orientation, the primitive cell translation vectors are $\tilde{\mathbf{u}}_i = \mathbf{u}_i$, see (2), and the shift vectors are $\boldsymbol{\mu}_i$, see (4). Inserting these vectors in (12), taking into account (13) and (14), the energies of five PSDs are expressed, as described below.

1. Case $S_m = AABB$, $S_k = BBAA$, see Fig. 3(b):

$$\begin{aligned}E &= \frac{1}{a^2} \left[4\omega_{AB}(R_1) - 4\Delta_{AB}(R_1) - 2\omega_{AB}(R_2) - 8\Delta_{AB}(R_3) \right. \\ &\quad - 8\omega_{AB}(R_4) + 16\omega_{AB}(R_5) + 8\Delta_{AB}(R_5) - 8\omega_{AB}(R_6) \\ &\quad + 12\omega_{AB}(R_7) - 12\Delta_{AB}(R_7) - 4\omega_{AB}(R_8) + 4\omega_{AB}(R_9) \\ &\quad \left. - 12\Delta_{AB}(R_9) - 24\omega_{AB}(R_{10}) \right].\end{aligned}\quad (16)$$

2. Case $S_m = AABB$, $S_k = ABAB$, see Fig. 3(c):

$$\begin{aligned}E &= \frac{1}{a^2} \left[\omega_{AB}(R_1) - 2\Delta_{AB}(R_1) - \omega_{AB}(R_2) + 2\omega_{AB}(R_3) \right. \\ &\quad - 4\Delta_{AB}(R_3) - 4\omega_{AB}(R_4) + 4\omega_{AB}(R_5) - 4\Delta_{AB}(R_5) \\ &\quad - 4\omega_{AB}(R_6) + 8\omega_{AB}(R_7) - 8\Delta_{AB}(R_7) - 2\omega_{AB}(R_8) \\ &\quad \left. + 5\omega_{AB}(R_9) - 6\Delta_{AB}(R_9) - 12\omega_{AB}(R_{10}) \right].\end{aligned}\quad (17)$$

3. Case $S_m = AABB$, $S_k = BABA$, see Fig. 3(d). The defect energy in this case is equal to the energy in case 2.

4. Case $S_m = AABB$, $S_k = ABBA$, see Fig. 3(e). The defect energy in this case is equal to the energy in case 2.

5. Case $S_m = AABB$, $S_k = BAAB$, see Fig. 3(f). The defect energy in this case is equal to the energy in case 2.

Note that the energies of all defects include the energy parameter Δ_{AB} since they change stoichiometry near the defect. In Case 1 NCAPB, and in Cases 2 to 5 C-domains with the same energy are realized.

6.2 Defects in the (100) Plane

For this defect orientation $\tilde{\mathbf{u}}_1 = \mathbf{u}_2$, $\tilde{\mathbf{u}}_2 = \mathbf{u}_3$, $\tilde{\mathbf{u}}_3 = \mathbf{u}_1$, see (2), and $\boldsymbol{\mu}_i$ are given by (4). Inserting these vectors in (12), the following results can be obtained for different domains of the $L1_0$ structure on both sides of the defect.

1. Case $S_m = ABAB$, $S_k = BABA$, see Fig. 4(b):

$$\begin{aligned}E &= \frac{1}{a^2} \left[-2\omega_{AB}(R_2) + 8\omega_{AB}(R_3) - 8\omega_{AB}(R_4) - 8\omega_{AB}(R_6) \right. \\ &\quad \left. + 16\omega_{AB}(R_7) - 4\omega_{AB}(R_8) + 16\omega_{AB}(R_9) - 24\omega_{AB}(R_{10}) \right].\end{aligned}\quad (18)$$

2. Case $S_m = ABAB$, $S_k = AABB$, see Fig. 4(c):

$$\begin{aligned}E &= \frac{1}{a^2} \left[\omega_{AB}(R_1) + 2\Delta_{AB}(R_1) - \omega_{AB}(R_2) + 2\omega_{AB}(R_3) \right. \\ &\quad - 4\Delta_{AB}(R_3) - 4\omega_{AB}(R_4) + 4\omega_{AB}(R_5) + 4\Delta_{AB}(R_5) \\ &\quad - 4\omega_{AB}(R_6) + 8\omega_{AB}(R_7) + 8\Delta_{AB}(R_7) - 2\omega_{AB}(R_8) \\ &\quad \left. + 5\omega_{AB}(R_9) + 6\Delta_{AB}(R_9) - 12\omega_{AB}(R_{10}) \right].\end{aligned}\quad (19)$$

3. Case $S_m = ABAB$, $S_k = BBAA$, see Fig. 4(d):

$$\begin{aligned}E &= \frac{1}{a^2} \left[\omega_{AB}(R_1) - 2\Delta_{AB}(R_1) - \omega_{AB}(R_2) + 2\omega_{AB}(R_3) \right. \\ &\quad - 4\Delta_{AB}(R_3) - 4\omega_{AB}(R_4) + 4\omega_{AB}(R_5) - 4\Delta_{AB}(R_5) \\ &\quad - 4\omega_{AB}(R_6) + 8\omega_{AB}(R_7) - 8\Delta_{AB}(R_7) - 2\omega_{AB}(R_8) \\ &\quad \left. + 5\omega_{AB}(R_9) - 6\Delta_{AB}(R_9) - 12\omega_{AB}(R_{10}) \right].\end{aligned}\quad (20)$$

4. Case $S_m = ABAB$, $S_k = ABBA$, see Fig. 4(e):

$$\begin{aligned}E &= \frac{1}{a^2} \left[-\omega_{AB}(R_2) + 4\omega_{AB}(R_3) - 4\omega_{AB}(R_4) - 4\omega_{AB}(R_6) \right. \\ &\quad \left. + 8\omega_{AB}(R_7) - 2\omega_{AB}(R_8) + 8\omega_{AB}(R_9) - 12\omega_{AB}(R_{10}) \right].\end{aligned}\quad (21)$$

5. Case $S_m = ABAB$, $S_k = BAAB$, see Fig. 4(f). The result is the same as in case 4.

Note that in Case 1 the defect energy is expressed through the ordering energies ω_{AB} , that is, CAPB is realized which does not change the stoichiometry near the defect. In Cases 4 and 5 the defect energy is also expressed in terms of ω_{AB} . These are the C-domains that do not change the stoichiometry near the defect. Interestingly, the energy of the defect in Case 1, Eq. (18), is exactly twice that of the defects in Cases 4 and 5, Eq. (21). Defects in Cases 2 and 3 give the energies in terms of both ω_{AB} and Δ_{AB} since they change the stoichiometry in the vicinity of the defects.

7 List of all Possible Planes of CAPBs in $L1_0$ Alloys

CAPBs are formed in ordered alloys by glide of partial dislocations, which leads to hardening of the alloy. CAPBs are created only by the dislocations whose Burger's vector is not a translation vectors of the superstructure [14]. To determine active slip systems in ordered alloys, it is important to know in which crystallographic planes CAPBs are possible.

To solve this problem, consider the superstructure $L1_0$, whose primitive translational cell is shown in Fig. 5. The primitive cell of the fcc lattice L^P has the following translation vectors, see Fig. 5:

$$\mathbf{v}_1 = (2, 0, 0), \quad \mathbf{v}_2 = (1, 1, 0), \quad \mathbf{v}_3 = (0, 1, 1). \quad (22)$$

The lattice L is then defined by the following generating vectors:

$$\begin{aligned} \mathbf{w}_1 = \mathbf{v}_1 = (2, 0, 0), \quad \mathbf{w}_2 = \mathbf{v}_2 = (1, 1, 0), \\ \mathbf{w}_3 = 2\mathbf{v}_3 = (0, 2, 2). \end{aligned} \quad (23)$$

The vectors \mathbf{w}_i are shown in Fig. 5 in orange. The translational cell defined by these vectors includes two atoms. In addition to (2-5) the $L1_0$ superstructure can be defined based on the lattice L :

$$Q = \bigcup_{m=1}^2 (L + \boldsymbol{\theta}_m)_{S_m}, \quad (24)$$

where the shift vectors of the monatomic lattice L are:

$$\boldsymbol{\theta}_1 = (0, 0, 0), \quad \boldsymbol{\theta}_2 = (0, 1, 1). \quad (25)$$

The sorts of the shifted lattices in (24) are:

$$S_1 = A, \quad S_2 = B. \quad (26)$$

As mentioned above, CAPB is obtained by the shift of a half of the crystal by the lattice vector \mathbf{t} which satisfies two conditions: (i) vector \mathbf{t} is parallel to the PSD plane (h, k, l) and (ii) it changes the sorts of atoms on sublattices. Such a vector is called an antiphase vector. The $L1_0$ superstructure defined by (24) and (26) includes 2 sublattices with the shift vectors $\boldsymbol{\theta}_m$. Displacement along $\boldsymbol{\theta}_2$ leads to a change in the sorts of atoms on the sublattices. Therefore, there is only one antiphase vector that creates PSDs:

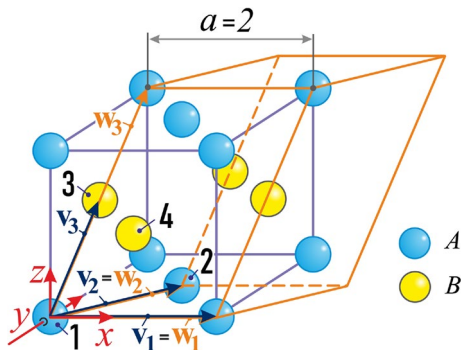


Fig. 5 Primitive translational cell of the fcc lattice defined by the vectors $\mathbf{v}_1, \mathbf{v}_2, \mathbf{v}_3$ and primitive translational cell of the $L1_0$ superstructure defined by the vectors $\mathbf{w}_1, \mathbf{w}_2, \mathbf{w}_3$

$$\mathbf{t} = \boldsymbol{\theta}_2 = (0, 1, 1). \quad (27)$$

The antiphase vector \mathbf{t} in (27) is given in the Cartesian coordinates. The calculations will be carried out in the basis of the vectors $\mathbf{v}_i, i = 1, 2, 3$, see (22), generating the fcc lattice L^P . In this basis, the antiphase vector \mathbf{t} is:

$$\mathbf{t} = (0, 0, 1) \stackrel{def}{=} (t_1, t_2, t_3). \quad (28)$$

The displacement vector (28) generates an infinite number of CAPB planes parallel to this vector. Moreover, the points of the lattice L can be shifted to the points $L + \mathbf{t}$ by any of the displacement vector of the form

$$(t_1 + \xi K_1, t_2 + \eta K_2, t_3 + \varphi K_3) \stackrel{def}{=} (a, b, c), \quad (29)$$

where ξ, η , and φ are arbitrary integers. CAPBs are formed in the plane with Miller's indices (h, k, l) parallel to at least one of the vectors in (29). Such Miller's indices can be found from the equation

$$ah + bk + cl = 0. \quad (30)$$

The integer solution of equation (30) having integer coefficients can be written in the form

$$\begin{pmatrix} h \\ k \\ l \end{pmatrix} = \begin{pmatrix} -bc(\alpha + \beta) \\ ac\alpha \\ ab\beta \end{pmatrix}, \quad (31)$$

where new integer parameters α and β are introduced. Inserting in (31) the coefficients a, b , and c defined in (29), the desired Miller indices can be written as:

$$\begin{pmatrix} h \\ k \\ l \end{pmatrix} = \begin{pmatrix} -(t_2 + \eta K_2)(t_3 + \varphi K_3)(\alpha + \beta) \\ (t_1 + \xi K_1)(t_3 + \varphi K_3)\alpha \\ (t_1 + \xi K_1)(t_2 + \eta K_2)\beta \end{pmatrix} = \begin{pmatrix} -\eta(1 + 2\varphi)(\alpha + \beta) \\ \xi(1 + 2\varphi)\alpha \\ \xi\eta\beta \end{pmatrix}. \quad (32)$$

To find all possible planes of CAPBs for the antiphase vector \mathbf{t} one should go through all the integer indices $\xi, \eta, \varphi, \alpha$, and β in equation (32). Note that in (32) $K_1 = 1, K_2 = 1, K_3 = 2$, as seen in (23). In practice, planes with small Miller indices are of interest, and they can be found by considering $-N < \xi, \eta, \varphi, \alpha, \beta < N$, where N is large enough.

Recall that the Miller indices in (32) are given in the basis \mathbf{v}_i . They can be converted into indices (h', k', l') with respect to the Cartesian coordinates using the following expressions:

$$(h', k', l') = \left(\frac{V_1}{V}, \frac{-V_2}{V}, \frac{V_3}{V} \right), \quad (33)$$

where the determinants of the following matrices must be calculated:

$$V = \begin{vmatrix} v_{11} & v_{12} & v_{13} \\ v_{21} & v_{22} & v_{22} \\ v_{31} & v_{32} & v_{33} \end{vmatrix}, \quad V_1 = \begin{vmatrix} v_{12} & v_{13} & h \\ v_{22} & v_{23} & k \\ v_{32} & v_{33} & l \end{vmatrix},$$

$$V_2 = \begin{vmatrix} v_{11} & v_{13} & h \\ v_{21} & v_{23} & k \\ v_{31} & v_{33} & l \end{vmatrix}, \quad V_3 = \begin{vmatrix} v_{11} & v_{12} & h \\ v_{21} & v_{22} & k \\ v_{31} & v_{32} & l \end{vmatrix}.$$

Here v_{ij} are given in the Cartesian coordinate system.

The complete list of planes where CAPBs are possible is (only planes with Miller indices (h' , k' , l') not greater than 2 are presented):

$$\begin{aligned} (0\ 1\ 0), & \quad (0\ 1\ 1), & (0\ 1\ 2), & (0\ 1\ \bar{1}), & (0\ 1\ \bar{2}), \\ (1\ 0\ 0), & (1\ 0\ 1), & (1\ 0\ 2), & (1\ 0\ \bar{1}), & (1\ 0\ \bar{2}), \\ (1\ 1\ 1), & (1\ 1\ \bar{1}), & (1\ 2\ 0), & (1\ 2\ 1), & (1\ 2\ 2), \\ (1\ 2\ \bar{1}), & (1\ 2\ \bar{2}), & (1\ \bar{1}\ 1), & (1\ \bar{1}\ \bar{1}), & (1\ \bar{2}\ 0), \\ (1\ \bar{2}\ 1), & (1\ \bar{2}\ 2), & (1\ \bar{2}\ \bar{1}), & (1\ \bar{2}\ \bar{2}), & (2\ 1\ 0), \\ (2\ 1\ 1), & (2\ 1\ 2), & (2\ 1\ \bar{1}), & (2\ 1\ \bar{2}), & (2\ \bar{1}\ 0), \\ & (2\ \bar{1}\ 1), & (2\ \bar{1}\ 2), & (2\ \bar{1}\ \bar{1}), & (2\ \bar{1}\ \bar{2}). \end{aligned} \quad (34)$$

8 Discussion

The results obtained should be discussed from a practical point of view.

In this work, a crystallographic analysis of alloys with the $L1_0$ superstructure was carried out and the sublimation energy of the alloy and the energy of the planar superstructure defect were derived analytically. The expression (32) was derived to find all possible planes where CAPBs are possible.

All possible domains (arrangements of A and B atoms on shifted cubic lattices) in the $L1_0$ superstructure are presented in Fig. 2. Any PSD separates two different domains. Since there are six such domains, there are at most 15 PSDs for any particular orientation, because there are 15 combinations of different domain pairs.

The list of all planes where CAPBs are possible, Eq. (34), is useful for the analysis of slip systems in the considered alloys. In fcc crystals, slip occurs on the close-packed $\{111\}$ planes along the close-packed $\langle 110 \rangle$ directions. There are 12 slip systems in total, since in each of the four octahedral planes $(1\ 1\ 1)$, $(1\ 1\ \bar{1})$, $(1\ \bar{1}\ 1)$, $(1\ \bar{1}\ \bar{1})$ there are three close packed directions. However, all these planes are in the list Eq. (34). Therefore, slip in all close-packed planes is hindered by the formation of CAPB. Then, the secondary slip systems experimentally observed for fcc crystals [43, 44], can become active. Indeed, for the slip system $\{001\}[110]$, CAPBs are formed in the planes $(1\ 0\ 0)$ and $(0\ 1\ 0)$, but they are not formed in the plane $(0\ 0\ 1)$. The dislocations can

easily slide in the latter plane. Similarly, for the slip system $\{110\}[110]$, CAPBs are formed in the planes $(0\ 1\ 1)$, $(0\ 1\ \bar{1})$, $(1\ 0\ 1)$ and $(1\ 0\ \bar{1})$, but they are not formed in the planes $(1\ 1\ 0)$ and $(1\ \bar{1}\ 0)$. Dislocation glide in the last two planes is not suppressed by the formation of CAPB.

Analytical expression for the energy of PSD, Eqs. (12)-(14), was obtained under several important assumptions: (i) the tetragonality of $L1_0$ alloys was not taken into account, (ii) pairwise interatomic interactions were assumed, and (iii) the relaxation of atoms near defects was not taken into account. This means that the obtained results are most reliable for alloys with small tetragonality and small deviation of elastic constants from the Cauchy relation, which is often used as a measure of the importance of the many-body part of potentials [45].

Nevertheless, the analytical expressions for PSD energy can be useful. For example, analysis of the defect energies for the $(1\ 0\ 0)$ plane reveals that the energy of the defect in Case 1, Eq. (18), is exactly twice that of the defects in Cases 4 and 5, Eq. (21).

Our crystallographic approach does not take into account the effect of temperature on the mechanical properties of ordered alloys. This problem can be solved using molecular dynamics or other methods.

9 Conclusions

The results of this study can be summarized as follows.

- An analysis of the translational and point symmetry of the $L1_0$ superstructure revealed all possible domains shown in Fig. 2. There are six such domains, and therefore, for any particular orientation, there are no more than 15 PSDs, according to the number of different combinations of domain pairs.
- An analytical expression (32) is obtained to find all possible CAPB orientations. The list of all planes on which CAPBs are possible, with Miller indices not higher than 2, is given by Eq. (34). This list is useful for analyzing slip systems in the alloys under consideration.
- Within the framework of the accepted assumptions, an analytical expression for the PSD energy, Eqs. (12)-(14), is obtained. Knowing the PSD energies, one can predict their probability: the most probable are defects with lower energy.

Overall, the results obtained are useful in the analysis of the impact of planar superstructure defects on mechanical and physical properties of the alloys with $L1_0$ superstructure.

Acknowledgements E.A.K. acknowledges the financial support of the Russian Science Foundation, grant No. 21-12-00275. The work

was supported within the framework of work on the State task of the Ministry of Science and Higher Education of the Russian Federation for USATU (agreement No. 075-03-2021-014/4) in youth research laboratory “Metals and Alloys under Extreme Impacts” and the grant NSH-4320.2022.1.2. For A.A.K. this work was supported by the Bashkir State Medical University Strategic Academic Leadership Program (PRIORITY-2030). S.V.D. acknowledges the support of the Grant NSH-4320.2022.1.2 of the President of the Russian Federation for state support of young Russian scientists - candidates of sciences and doctors of sciences.

Declarations

Conflict of interest statement The authors declare no conflict of interest.

References

1. A. Kohn, N. Tal, A. Elkayam, A. Kovács, D. Li, S. Wang, S. Ghanad-zadeh, T. Hesjedal, R. Ward, *Appl. Phys. Lett.* **102**(6), 062403 (2013). <https://doi.org/10.1063/1.4791576>
2. G. Varvaro, S. Laureti, D. Fiorani, J. Magn. Magn. Mater. **368**, 415–420 (2014). <https://doi.org/10.1016/j.jmmm.2014.04.058>
3. Y. Liu, U. Bierbrauer, C. Seick, S.T. Weber, M. Hofherr, N.Y. Schmidt, M. Albrecht, D. Steil, S. Mathias, H.C. Schneider, B. Rethfeld, B. Stadtmüller, M. Aeschlimann, Ultrafast magnetization dynamics of Mn-doped $L1_0$ FePt with spatial inhomogeneity. *J. Magn. Magn. Mater.* **502**, 166477 (2020). <https://doi.org/10.1016/j.jmmm.2020.166477>
4. N. Sriplai, S. Koowattanasuchat, P. Kidkhunthod, N. Chanlek, S.J. Eichhorn, S. Pinitsoontorn, *J. Alloy. Compd.* **739**, 19–29 (2018). <https://doi.org/10.1016/j.jallcom.2017.12.202>
5. S. Kumar, K. Sharma, G. Sharma, A. Gupta, V. Raghavendra Reddy, A. Gome, S.C. Das, *Mater. Today. Proc.* **60**, 945–948 (2022). <https://doi.org/10.1016/j.matpr.2021.11.222>
6. Y.-C. Lin, C.-F. Lin, *IEEE T. Magn.* **51**(11), 7145448 (2015). <https://doi.org/10.1109/TMAG.2015.2451952>
7. W. Tian, T. Sano, M. Nemoto, *Philos. Mag. A* **68**(5), 965–976 (1993). <https://doi.org/10.1080/01418619308219379>
8. M. Kostenko, J. Li, Z. Zeng, Y. Zhang, S. Sharf, A. Gusev, A. Lukoyanov, *J. Alloy. Compd.* **891**, 162063 (2022). <https://doi.org/10.1016/j.jallcom.2021.162063>
9. Y. Zhao, S. Yuan, Q. Chang, Z. Zhou, D. Kou, W. Zhou, Y. Qi, S. Wu, *Adv. Funct. Mater.* **31**(10), 2007928 (2021). <https://doi.org/10.1002/adfm.202007928>
10. J. Goiri, A. Van Der Ven, *Phys. Rev. B* **94**(9), 094111 (2016). <https://doi.org/10.1103/PhysRevB.94.094111>
11. D. Zhao, L. Chang, X. Wang, K. Liu, Q. Wang, Z. Sun, C. Liu, J. Wang, Q. Wang, W. Pei, *New. J. Chem.* **46**(14), 6747–6755 (2022). <https://doi.org/10.1039/d2nj00337f>
12. Z. Sun, D. Zhao, X. Wang, M. Yan, L. Chang, Q. Wang, W. Pei, *J. Alloy. Compd.* **870**, 159384 (2021). <https://doi.org/10.1016/j.jallcom.2021.159384>
13. W. Pei, D. Zhao, C. Wu, Z. Sun, C. Liu, X. Wang, J. Zheng, M. Yan, J. Wang, Q. Wang, *ACS Appl. Nano. Mater.* **3**(2), 1098–1103 (2020). <https://doi.org/10.1021/acsnm.9b02420>
14. R. Kikuchi, J. Cahn, *Acta. Metall.* **27**(8), 1337–1353 (1979). [https://doi.org/10.1016/0001-6160\(79\)90203-7](https://doi.org/10.1016/0001-6160(79)90203-7)
15. Y. Le Bouar, A. Loiseau, A. Finel, *Phys. Rev. B* **68**(22), 224203 (2003). <https://doi.org/10.1103/PhysRevB.68.224203>
16. G. Hug, A. Loiseau, P. Veysseyre, *Philos. Mag. A* **57**(3), 499–523 (1988). <https://doi.org/10.1080/01418618808204682>
17. S. Bahamida, A. Fnidiki, M. Coisson, G. Barrera, F. Celegato, E. Olivetti, P. Tiberto, A. Laggoun, M. Boudissa, *Thin Solid Films* **668**, 9–13 (2018). <https://doi.org/10.1016/j.tsf.2018.10.013>
18. R. Voskoboinikov, *Nucl. Instrum. Meth. B* **460**, 92–97 (2019). <https://doi.org/10.1016/j.nimb.2019.04.080>
19. F. Bittner, J. Freudenberger, L. Schultz, T. Woodcock, *J. Alloy. Compd.* **704**, 528–536 (2017). <https://doi.org/10.1016/j.jallcom.2017.02.028>
20. S. Zhang, W. Qi, B. Huang, *J. Chem. Phys.* **140**(4), 044328 (2014). <https://doi.org/10.1063/1.4863350>
21. G. Varvaro, P. Imperatori, S. Laureti, C. Cannas, A. Ardu, P. Plescia, A. Capobianchi, *J. Alloy. Compd.* **846**, 156156 (2020). <https://doi.org/10.1016/j.jallcom.2020.156156>
22. O. Seo, J.Y. Lee, J.M. Kim, J.-W. Kim, H.C. Kang, J. Chung, D.Y. Noh, *J. Alloy. Compd.* **666**, 232–236 (2016). <https://doi.org/10.1016/j.jallcom.2016.01.069>
23. S.I. Konorev, R. Kozubski, M. Albrecht, I.A. Vladymyrskiy, *Comp. Mater. Sci.* **192**, 110337 (2021). <https://doi.org/10.1016/j.commatsci.2021.110337>
24. P. Rani, M.K. Kashyap, R. Singla, J. Thakur, A.H. Reshak, *J. Alloy. Compd.* **835**, 155325 (2020). <https://doi.org/10.1016/j.jallcom.2020.155325>
25. C. Frommen, H. Rösner, *Mater. Lett.* **58**(1–2), 123–127 (2004). [https://doi.org/10.1016/S0167-577X\(03\)00428-2](https://doi.org/10.1016/S0167-577X(03)00428-2)
26. M. Ohno, T. Mohri, *Philos. Mag.* **83**(3), 315–328 (2003). <https://doi.org/10.1080/0141861021000039446>
27. T. Mohri, M. Ohno, Y. Chen, *J. Phase Equilib. Diff.* **27**(1), 47–53 (2006). <https://doi.org/10.1361/105497106X92790>
28. T. Mohri, *Comp. Mater. Sci.* **49**(4, Suppl.), S181–S186 (2010). <https://doi.org/10.1016/j.commatsci.2010.02.001>
29. R. Kozubski, M. Kozłowski, J. Wrobel, T. Wejrzanowski, K. Kurzydłowski, C. Goyhenex, V. Pierron-Bohnes, M. Rennhofer, S. Malinov, *Comp. Mater. Sci.* **49**(1, Suppl.), S80–S84 (2010). <https://doi.org/10.1016/j.commatsci.2010.01.046>
30. I. Bacic, I. Franovic, M. Perc, *Europhys. Lett.* **120**, 68001 (2017). <https://doi.org/10.1209/0295-5075/120/68001>
31. M.D. Starostenkov, S.V. Dmitriev, A.V. Bakaldin, *Russ. Phys. J.* **36**, 242–246 (1993). <https://doi.org/10.1007/BF00559628>
32. M.D. Starostenkov, S.V. Dmitriev, S.I. Golobokova, *Russ. Phys. J.* **35**, 456–460 (1992). <https://doi.org/10.1007/BF00558858>
33. K. Khromov, I. Pankratov, V. Vaks, *Phys. Rev. B* **72**(9), 094207 (2005). <https://doi.org/10.1103/PhysRevB.72.094207>
34. P.S. Ghosh, A. Arya, U.D. Kulkarni, G.K. Dey, S. Hata, T. Nakano, K. Hagihara, H. Nakashima, *Philos. Mag.* **94**(11), 1202–1218 (2014). <https://doi.org/10.1080/14786435.2014.885135>
35. U.D. Kulkarni, S. Hata, T. Nakano, M. Mitsuhara, K. Ikeda, H. Nakashima, *Philos. Mag.* **91**(22), 3068–3078 (2011). <https://doi.org/10.1080/14786435.2011.563761>
36. J.W. Cahn, R. Kikuchi, *J. Phys. Chem. Solids* **27**(8), 1305–1317 (1966). [https://doi.org/10.1016/0022-3697\(66\)90015-1](https://doi.org/10.1016/0022-3697(66)90015-1)
37. M.A. Krivoglaз, A.A. Smirnov, *The Theory of Order-Disorder in Alloys* (Mac Donald, London, 1984)
38. M.D. Starostenkov, A.M. Kirienko, *Phys. Status Solidi A* **142**(2), 321–330 (1994). <https://doi.org/10.1002/pssa.2211420204>
39. A.R. Khalikov, M.D. Starostenkov, E.A. Korznikova, E.A. Sharapov, S.V. Dmitriev, *Intermetallics* **137**, 107276 (2021). <https://doi.org/10.1016/j.intermet.2021.107276>
40. M.D. Starostenkov, S.V. Dmitriev, O.K. Starostenkova, *J. Struct. Chem.* **38**, 930–935 (1997). <https://doi.org/10.1007/BF02763812>
41. Y.I. Sirotnin, M.P. Shaskolskaya, *Fundamentals of Crystal Physics* (Mir Publishers, Moscow, 1982)
42. S.A. Shcherbinin, K.A. Krylova, G.M. Chechin, E.G. Soboleva, S.V. Dmitriev, *Commun. Nonlinear Sci. Numer. Simul.* **104**, 106039 (2022). <https://doi.org/10.1016/j.cnsns.2021.106039>
43. M. Carrard, J. Martin, *Philos. Mag. A* **56**(3), 391–405 (1987). <https://doi.org/10.1080/01418618708214395>

44. M. Carrard, J. Martin, *Philos. Mag. A* **58**(3), 491–505 (1988). <https://doi.org/10.1080/01418618808210426>
45. E.V. Zarochentsev, E.P. Troitskaya, V.V. Chabanenko, *Phys. Solid. State*. **46**, 249 (2004). <https://doi.org/10.1134/1.1649419>

Publisher's Note Springer Nature remains neutral with regard to jurisdictional claims in published maps and institutional affiliations.

Springer Nature or its licensor holds exclusive rights to this article under a publishing agreement with the author(s) or other rightsholder(s); author self-archiving of the accepted manuscript version of this article is solely governed by the terms of such publishing agreement and applicable law.